Engineering Science and Technology, an International Journal 57 (2024) 101819

Contents lists available at ScienceDirect

Engineering Science and Technology, an International Journal

journal homepage: www.elsevier.com/locate/jestch

A planar-structured circularly polarized single-layer MIMO antenna for wideband millimetre-wave applications

Ubaid Ullah [a,*], Slawomir Koziel [b,c], Anna Pietrenko-Dabrowska [c], Shahanawaz Kamal [d]

[a] Networks and Communication Engineering Department, Al Ain University, P.O. Box (112612), Abu Dhabi, UAE
[b] Engineering Optimization and Modeling Center of Reykjavik University, Reykjavik, Iceland
[c] Faculty of Electronics, Telecommunications and Informatics, Gdansk University of Technology, 80- 233 Gdansk, Poland
[d] Radio Frequency Design Enablement Group, Barkhausen Institut, 01067 Dresden, Germany

ARTICLE INFO

Keywords:
Millimeter-wave communication
EM-driven design
Circularly polarized antennas
Wideband Antenna

ABSTRACT

This paper presents a planar multiple-input-multiple-output (MIMO) antenna with dual circular polarization (CP) and a simple geometry for millimetre-wave band. The proposed design is featuring a fully grounded coplanar waveguide (CPW) and a systematically perturbed feedline radiator. The symmetry of the electric field is disrupted using varying stub sizes and offsets between the stubs, resulting in wideband operation and circularly polarized waves. Following full optimization of the physical parameters, the numerical design is validate experimentally. The results indicate that the proposed antenna design achieves a −10 dB impedance bandwidth from 24.6 GHz to 32.1 GHz, with an axial ratio (AR) of 3 dB or less from 26 GHz to 31.8 GHz. The peak realized gain is 10.3 dBic, with steady broadside radiation. The envelope correlation coefficient (ECC) is 0.01, and the diversity gain is 10 dB across the operating band. The planar structure and the wideband performance of the proposed design makes it suitable for application necessitating fix beam applications in the mm-wave band.

1. Introduction

Multiple-input-multiple-output (MIMO) technology has been a key factor in the recent exponential growth of forthcoming wireless communication technology. With the expansion of the spectrum to the millimeter-wave band, the need for improving the hardware to meet the extremely high data rate requirements has grown rapidly [1,2]. MIMO technology has been successfully deployed in the 5G mid-band, which has shown promising results specifically in the sub-6 GHz band [3–7]. Due to longer wavelengths and low propagation losses in the mid-band, a balanced spectrum capacity and wider coverage can be established. On the contrary, the millimeter wave band suffers from propagation losses and high attenuation as the signal dies faster when propagating and penetrating through different media. The multi-tier network envisions the mm-wave 5G networks which include machine-to-machine (M2M) communication [8], Tactile Internet [9], vehicle-to-vehicle (V2V) communication [10], as well as vehicle-to-infrastructure (V2I) communication [11]. Withholding the signal integrity in the complex network architecture is challenging due to the transmission being conducted at very high frequencies compared to the traditional low-frequency networks [12,13]. High-gain antenna arrays with circular polarization (CP) are indispensable to overcome the high attenuation issue of the signal and maintain reliable information transfer over wireless networks. The array structure allows for reducing the propagation losses without the need for additional power [2,11,14,15]. Utilizing high-gain MIMO array antenna systems in the mm-wave band could easily serve as a backbone for highly efficient wireless communications.

Wideband antenna arrays with unidirectional radiation pattern are essential for modern wireless communication systems especially in the mm-wave band [16]. Multiple applications including 5G, the Internet-of-things, satellite communication, and automotive radar applications in this band requires the ability to deliver high data rates with focused beams to improve the efficiency of the system. Their directional nature of these antenna decreases the multipath effects and maintains relatively high signal integrity [17,18].

In this paper, a single-layer series-fed linear array antenna working through circular polarization is presented. The proposed antenna design is constructed on a single substrate coplanar waveguide-fed microstrip transmission line with asymmetrically placed short stubs on both sides

* Corresponding author.
E-mail addresses: ubaid.ullah@aau.ac.ae (U. Ullah), koziel@ru.is (S. Koziel), anna.dabrowska@pg.edu.pl (A. Pietrenko-Dabrowska), shahanawaz.kamal@barkhauseninstitut.org (S. Kamal).

https://doi.org/10.1016/j.jestch.2024.101819
Received 2 March 2024; Received in revised form 10 July 2024; Accepted 19 August 2024
Available online 29 August 2024

of the line. These magnetically coupled stubs provide a trail for the currents to flow along the sides of the small stubs enabling constructive correlation of the fields, therefore, energy is radiated in the free space. With the systematic alteration of the fringing electromagnetic fields effectively excites the orthogonal radiating fields in a wide spectrum of the frequency. The linear and planar nature of the series-fed array allows for easy implementation of the MIMO structure. In the proposed MIMO antenna, each port excites a different sense of circular polarization resulting in a highly isolated and independently working design. In addition to a simple structure, a wide impedance bandwidth of more than 25 %, stable gain, directional radiation pattern, and a minor envelope correlation coefficient (ECC) is achieved. The antenna maintains a lower than 3 dB axial ratio (AR) throughout the operating frequency bandwidth, which is highly desirable for CP based devices.

2. Antenna design and operating mechanism

2.1. Antenna design

The detailed geometrical configuration of the presented array MIMO antenna has been shown in Fig. 1. A single Rogers 4003 substrate with thickness h_s = 0.508 mm and dielectric constant ε_r = 3.38 is used to implement the proposed MIMO antenna. A grounded coplanar waveguide (GCPW) with an extended feeding line is printed on top of the substrate as depicted in Fig. 1(a). The calculated gap g = 0.323 mm between the microstrip and the ground planes coplanar with feedline and width of the microstrip (Wm = 1.05 mm) is used for achieving 50-Ohm input impedance. Furthermore, two different-size stubs are placed asymmetrically on each side beside the extended length of the microstrip line. As illustrated, the magnetically coupled pair of stubs breaks the symmetry of the microstrip line fringing field, making it radiate effectively in the broadside direction. The enlarged section in Fig. 1(c) shows the physical dimensions and in-depth description of the single pair of stubs concerning the microstrip line. Fig. 1(b) shows the bottom of the substrate, which is fully laminated. The pair of stubs are extended to four elements placed half-guided-wavelength apart down the longitudinal dimension of the feedline. For realizing the MIMO design, the pair of stubs are reflected with respect to the feedline to achieve the different sense (LHCP and RHCP) of circular polarization. The antennas are designed on a shred ground plane at the backside of the substrate. All the physical dimensions are optimized simultaneously at the full-wave level of description and listed in Table 1.

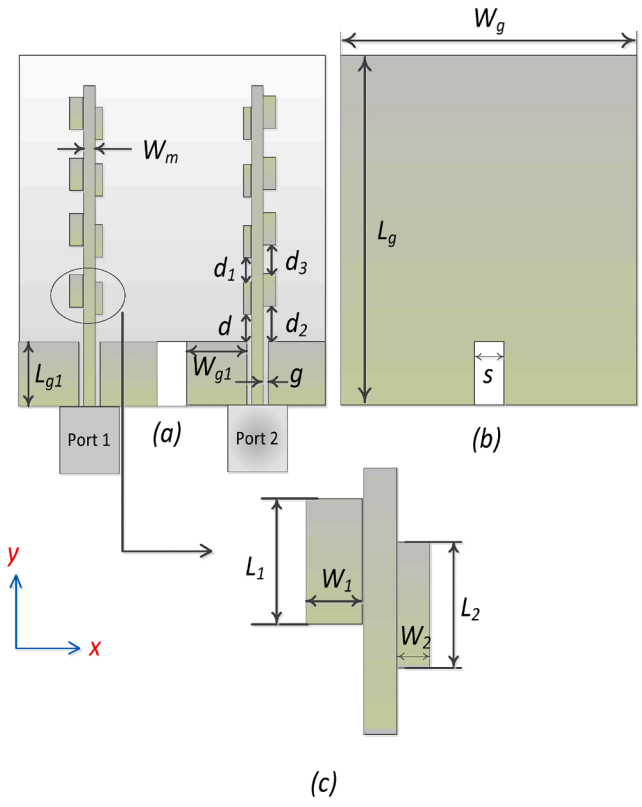

Fig. 1. Proposed structure of the linear series-fed microstrip array: (a) Top view, (b) bottom view, (c) parametric view of the asymmetrical stubs.

2.2. Operating principle and CP radiation mechanism

The operating mechanism of the antenna could be best explained using the transmission line theory. As the principal radiator of the proposed antenna is the microstrip line extended from GCPW, it is important to recall the behavior of the propagating electromagnetic fields along its length. As opposed to printed microstrip lines, in the GCPW, the electromagnetic fields are more concentrated between the strip line and the bottom ground plane of the substrate. The fringing electric field along the microstrip line exhibits a periodic pattern, reversing direction every half wavelength. This results in equivalent magnetic currents on each side with equal amplitudes but opposite directions. Due to this phase difference in the traveling periodic fields, they cancel each other as shown in Fig. 2. Systematic alteration of the microstrip line can break this symmetry of the fields by amplitude tapering. In the proposed design, the field distribution of the microstrip line is altered by using a magnetically coupled pair of stubs of different electrical sizes on both sides with a small offset. The presence of the small stubs effectively disrupt the balance of the electric and magnetic fields down the length of the feeding line. To ascertain wideband antenna operation, the approximate length of each stub is kept to half-guided wavelength calculated at 26 GHz and 29 GHz using equation (1) and (2). Where, ε_r is the relative dielectric constant, while the width of the microstrip line is *w* and is substrate thickness is *h*. This modification of the microstrip line geometry eliminates the dominant out-of-phase field components as depicted with the equivalent field distribution in Fig. 2(b), making the antenna radiate effectively. Moreover, with phase progression from 0 degrees to 360 degrees, the vector fields along the width of the stubs yield the perpendicular components required for the circular polarization. This is illustrated separately in Fig. 3 with the help of the simulated surface current on the numerical model of the antenna. For clarity, the simulated field distributions are shown on the stubs only. As seen in Fig. 3(a), at zero angular time, the horizontal components of the vector field in the x-direction are opposite to each other along the width of the stubs, therefore they can cancel each other. The fields along the negative y-direction are all in phase on both stubs which contribute to the vertical components of the radiated field. At 90 degrees, the orientation of the vector fields along the width of the stubs is all in the negative x-direction as depicted in Fig. 3(b), which adds up in phase and yields the horizontal components of the CP. On the other hand, the vertical components along the length of the stubs are in opposite directions resulting in field cancelation. Fig. 3(c) illustrates the surface vector fileds on the stubs at 180 degrees. The vector fields in both the horizontal and vertical directions are opposite to that of Fig. 1 (a). The in-phase vertical field is in the positive direction on both stubs while the horizontal fields along the width of the stubs are 180 degrees

Table 1
Optimized Parameter Values.

Parameter	Value	Parameter	Value	Parameter	Value
L_1	2.932	W_{g1}	5.652	d	2.5138
W_1	1.234	L_g	34.476	d_1	1.8610
L_2	3.265	W_g	31.360	d_2	3.3179
W_2	0.8293	L_m	30.163	d_3	2.2796
L_{g1}	6.557	W_m	1.050	s	5.6302

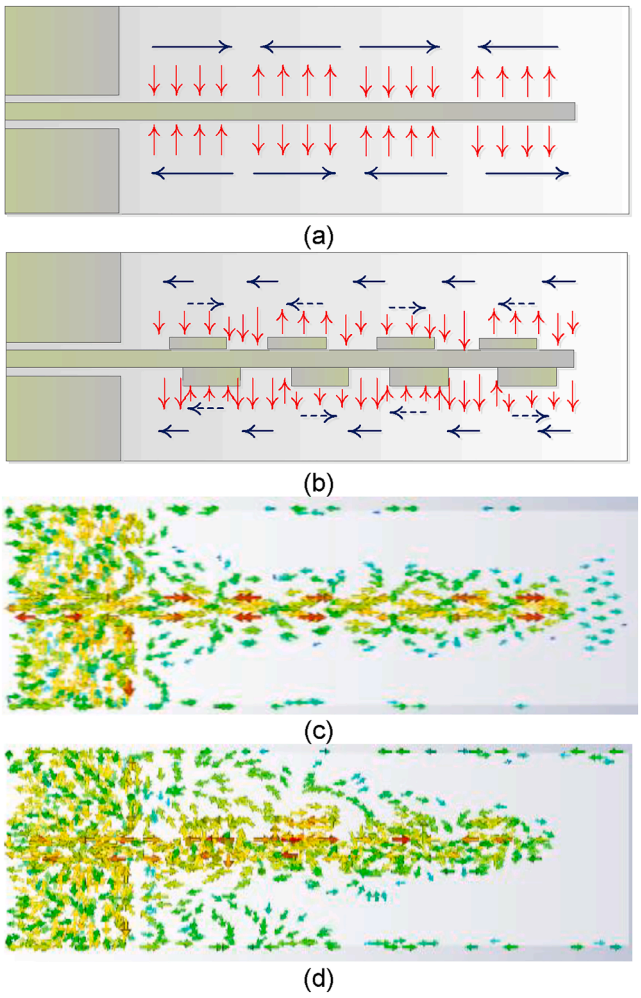

Fig. 2. Sketch of the Electric filed (red color) and magnetic field (blue color). (a) sketched field distribution of normal microstrip line, (b) sketched field distribution of the modified microstrip line, (c) simulated field distribution of normal microstrip line, (d) simulated field distribution of the modified microstrip line.

out-of-phase. Finally, the fields at 270 degrees are shown in Fig. 3(c).

As it can be (Table 2) observed, the field in the positive x-direction is in-phase, whereas the fields along the y-direction are out-of-phase. The horizontal fields contribute to circular polarization while the vertical fields cancel each other. The field vectors demonstrate a clockwise rotation with phase progression from 0 degrees to 360 degrees, generating right-hand circular polarization. To add further clarity to the concept, the major electric characteristics of the single antenna design are shown in Fig. 3 (e) and (f). The reflection coefficient of the antenna with symmetric fields and asymmetric fields shows that the antenna has a minor resonance for symmetric case which is ascribed to coplanar grounds. For the asymmetric case, the in-band reflection coefficient is less then – 10 dB. Likewise, the AR response of the antenna with symmetric and asymmetric fields is shown in Fig. 3 (e) which clearly reflects circular polarization with AR less than 3 dB.

$$\lambda_g = \frac{\lambda_o}{\sqrt{\varepsilon_{eff}}} \tag{1}$$

$$\varepsilon_{eff} = \frac{\varepsilon_r + 1}{2} + \frac{\varepsilon_r - 1}{2}\left(\frac{1}{\sqrt{1 + 12\frac{h}{w}}}\right) \tag{2}$$

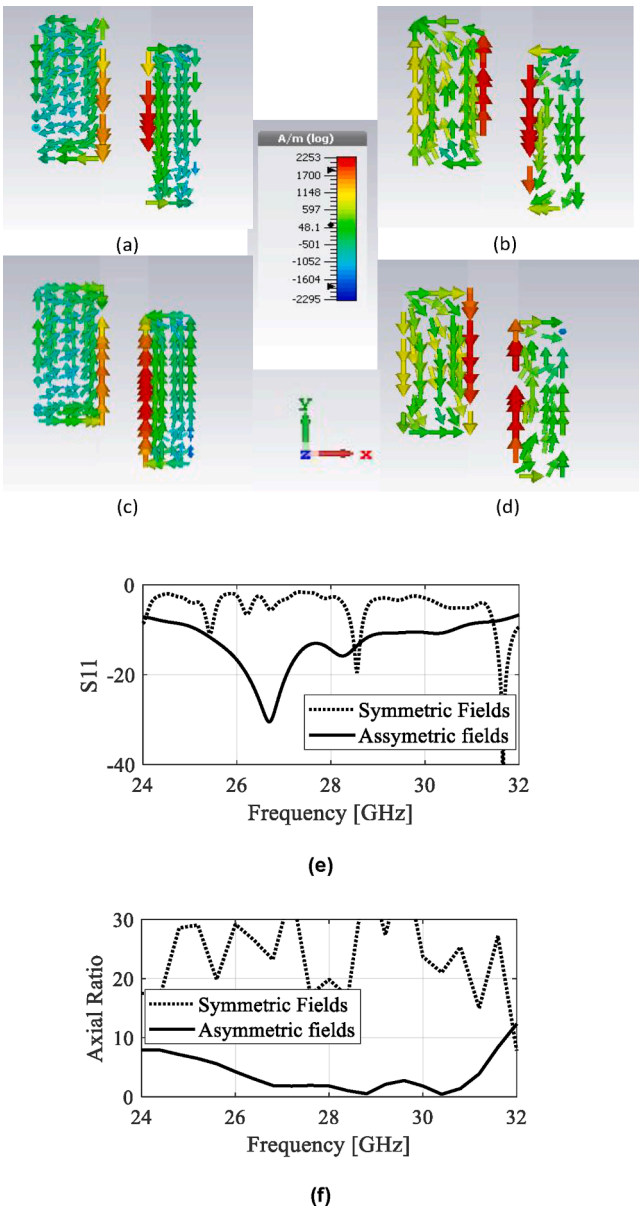

Fig. 3. Orientation of the current on the magnetically coupled asymmetrical placed stubs at different angular times: (a) 0°, (b) 90°, (c) 180°, (d) 270°, (e) Reflection coefficient, (f) Axial ratio.

3. Experimental validation

3.1. Analysis of the antenna S-parameters

The proposed antenna is fabricated following its full-wave analysis and optimization in CST Microwave Studio. The front and back view of the antenna prototype is shown in Fig. 4. The prototype is mounted with an end-launch connector for excitation of the antenna. Experimental characterization and validation of the numerical results are performed at Reykjavik University, Iceland. A photograph of the setup for practical characterization in the anechoic chamber is illustrated in Fig. 4 (c). Each port is characterized individually, with the other port terminated using the matched 50-Ohm load. The results in terms of simulated and measured curves of the S-parameters are depicted in Fig. 5 (a) and 5 (b), correspondingly. The measured value of the reflection coefficient indicates that the antenna retains $|S_{11}|$ value of less then –10 dB reference value from 24.6 GHz to approximately 32.1 GHz. The comparative

Table 2
Benchmark designs.

Ref.	Frequency (GHz)	Number of elements	% BW $\|S_{11}\|$	Substrate permittivity	LP/CP	Max gain	Size (L×W) ($\lambda_o \times \lambda_o$)
[19]	24.0	1	5	3.3	CP	8.5	7.59 × 1.09
[20]	28.0	1	8	2.2	CP	2.2	0.19 × 0.15
[21]	27.0	4	21.4	2.2	LP	12.18	2.70 × 0.90
[22]	28.0	1	16	3.3	CP	8.8	3.8 × 1.25
[23]	2.37	4	1.8	6.15	CP	9.8	––
[24]	28.0	12	33	2.2	LP	16.	8.97 × 1.87
Proposed	28.0	4	26.5	3.38	CP	10.3	2.8 × 0.94

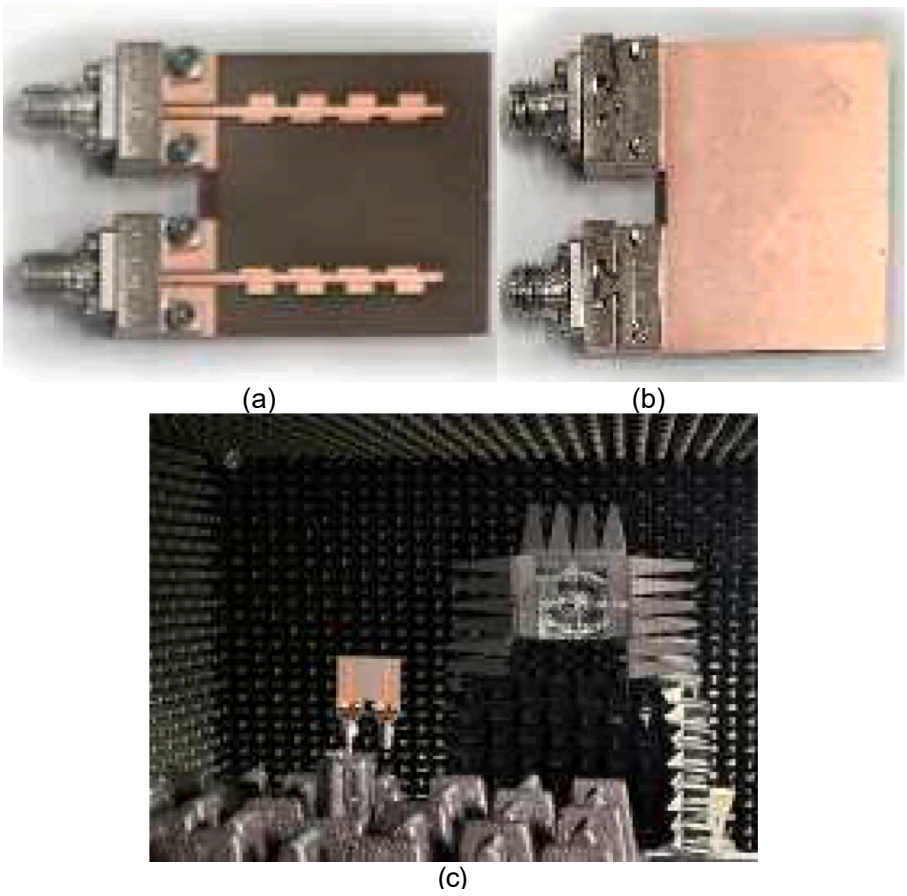

Fig. 4. Prototype of the proposed Antenna: (a) Top view, (b) bottom view, (c) Antenna prototype in the anechoic chamber.

impedance bandwidth of the antenna is 26.5 % with 28.35 GHz being the center frequency. This corroborates the wideband response of the proposed design. The simulated and measured isolation ($|S_{21}|$) has been depicted in Fig. 5 (b). The results show that the isolation $|S_{21}|$ between the two antennas is smaller then –25 dB indicating highly isolated MIMO ports. It is important to remember that the isolation of the port is a vital factor in high-performance MIMO antenna. In the proposed design, no additional decoupling methods are used. Excellent isolation is achieved due to the very geometrical structure of the antenna and the different sense of circular polarization of each port.

3.2. Axial ratio, realized gain, and radiation pattern

Axial ratio is another important electrical characteristic of any antenna radiating circularly polarized fields. The proposed design is characterized by AR analysis and the simulation and measure results are illustrated in Fig. 6(a). The simulation results show that the antenna has a wide 3 dB AR bandwidth in the range of 26 GHz to 32 GHz yielding approximately 21 % relative bandwidth. The measured results are slightly distorted and show the axial ratio less then 3 dB from 27 GHz to 31.8 GHz. It is important to mention here that at the mm-wave band, owing to short wavelengths, the axial ratio is extremely sensitive to minor changes in the physical parameters. The difference in the simulated and measured axial ratio is attributed to the fabrication tolerance of the antenna. The realized gain is evaluated in the direction of maximum radiation, which is slightly away from the broadside direction due to asymmetrical current distribution on the coupled stubs. The measured and simulated realized gain (RG) is shown in Fig. 6(b), which indicates a relatively steady gain across the bandwidth. The maximum gain of 10.3 dBic is achieved, with approximately 9.5 dBic of the average value over the operating bandwidth of the antenna. Finally, the radiation patterns of the antenna port 1 in the xz- and yz-planes are shown in Fig. 7 at two frequency points (27 GHz and 30 GHz) within the working band of the proposed design. The radiation pattern in the xz-plane is directed in the broadside direction, showing stable performance. On the other hand, the yz-plane pattern is shifted by a few degrees to the right

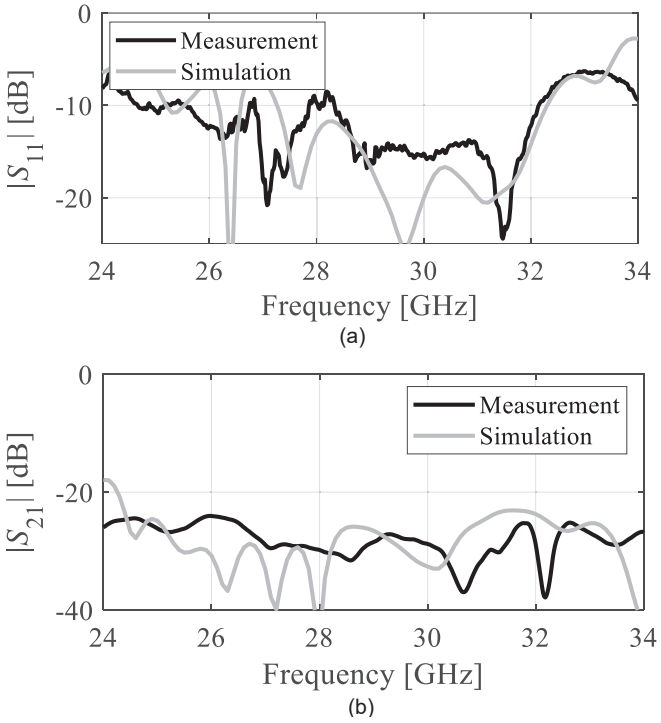

Fig. 5. Reflection coefficient and isolation; (a) S11, (a) S21.

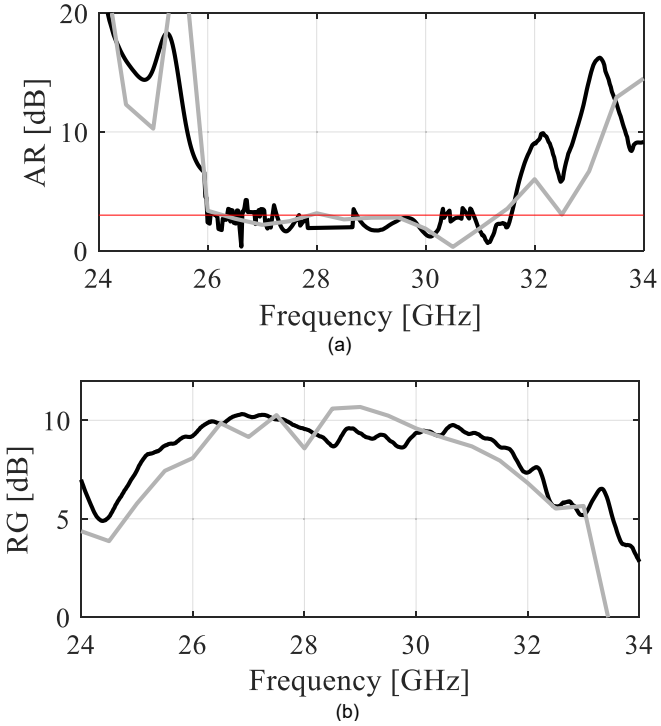

Fig. 6. Simulated (gray) and measured (black); (a) axial ratio, (b) Realized gain.

from the broadside direction, which is due to the broken symmetric filed distribution on the stubs. Overall, the proposed antenna maintains a stable radiation pattern throughout with slight discrepancies. The alteration between the co-polarization fields and cross-polarized fields is more than 10 dB in the maximum radiation direction, ensuring the applicability of the antenna under directional requirements. A small overlap between the cross-pols and the co-pols is observed which is due

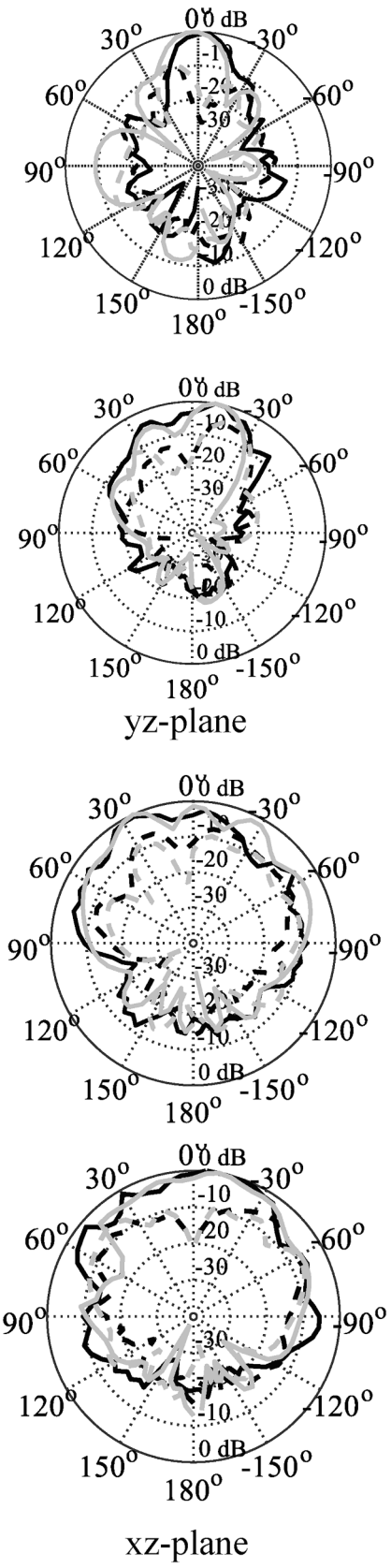

Fig. 7. Simulated radiation pattern (gray) and measured radiation pattern (black) yz- (top) and xz-plane (bottom), co-pol (—), cross-pol (– – –).

to the small finite ground plane which causes diffraction and reflection at the edges. The total power radiated by the antenna is 84 % to 88 % within the antenna operating bandwidth with the minimum first null bandwidth of 120°.

3.3. Envelop correlation coefficient and diversity gain

To further corroborate the performance of the proposed design, the envelop correlation coefficient and the diversity gain of the antenna are analyzed. Fig. 8 (a) shows the ECC of the antenna which is analyzed and calculated based on the farfield radiation patterns of the two antennas. The results indicate that from 24 GHz to 33 GHz, the maximum value of ECC is 0.01, which shows that the two antennas are almost entirely uncorrelated. Furthermore, the simulated diversity gain of the antenna is graphed in Fig. 8 (b). In MIMO antennas, diversity gain is a key metric, which is a function of multiple parameters including but not limited to spatial separation, frequency, elevation angle, etc. The proposed design shows a maximum level of diversity gain (~10 dB) throughout the antenna passband reflecting the high reliability of the device.

3.4. Antenna benchmarking

Table II shows a comprehensive benchmarking of the proposed antenna against the recent state-of-the-art planar antenna designs in terms of multiple performance figures. The comparison of these parameters demonstrates that the proposed structure outperforms other designs in multiple aspects. It is imperative to mention here that the literature offers several designs that exhibit better performance, cf. [3,7,12,13,25,26,27]. However, these antennas employ costly multilayer architectures and/or complex feeding mechanisms. In [28], a multilayer MIMO antenna was reported which is designed for 3.3 GHz and operates in a narrow impedance bandwidth. Similarly, in [29], a dielectric resonator MIMO antenna was reported which utilized aperture coupling and an overall bulky antenna design. Moreover, most of the above reference designs operate with a narrow impedance bandwidth and work with linear polarization. Conversely, the submitted design is executed on a single laminated substrate with a simple straightforward geometry, requiring no active elements for the simultaneous excitation of the orthogonal components required for circularly polarization. Furthermore, a size comparison is done at the center frequency using the calculated electrical size characteristics of the antenna dimensions in terms of the (free-space) wavelength. To ensure a fair assessment of the parameters, we compare the size of the proposed design with other design referenced in the table, which is mainly comprised of solitary antenna designs. It is important to highlight that the antenna described in [23] is notably reduced in physical size, as well as other electrical feature are not close to benchmarking with the design presented in this paper.

4. Conclusion

A printed microstrip line-based linear series array MIMO antenna that extends from a grounded coplanar waveguide has been studied in this study. The proposed design is realized by altering the fringing field on both sides of the microstrip line by systematically adding pairs of stubs on either sides of the feed-line radiator. The antenna is analyzed numerically at the full-wave EM simulation level and subsequently validated experimentally. Both the experimental and numerical results clearly illustrates that the proposed method yields a wideband circularly polarized antenna with a center frequency of ~ 29 GHz. Along with wideband response of the antenna, the proposed antenna retains a steady far-field pattern in the direction away from the antenna with almost level gain in the passband. Moreover, due to simple geometry, a changed sense of CP in the planar MIMO design is achieved ensuring high isolation and low levels of correlation between the antennas.

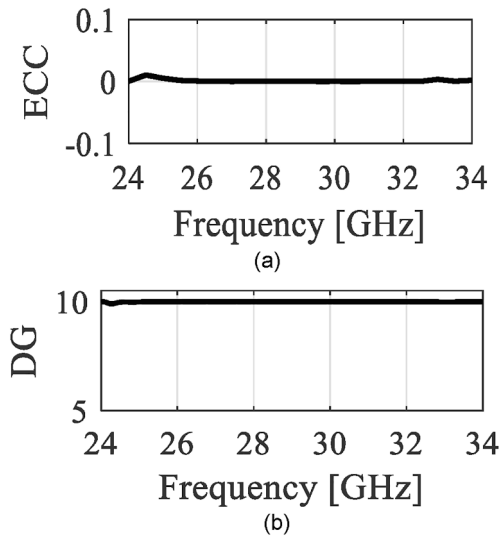

Fig. 8. (a) Simulated ECC, (b) Diversity gain.

CRediT authorship contribution statement

Ubaid Ullah: Writing – original draft, Methodology, Investigation, Formal analysis, Conceptualization. **Slawomir Koziel:** Supervision, Software, Resources, Project administration, Funding acquisition, Formal analysis. **Anna Pietrenko-Dabrowska:** Writing – review & editing, Visualization, Validation, Software. **Shahanawaz Kamal:** Writing – review & editing, Resources, Methodology, Investigation, Data curation.

Acknowledgment

This work was supported in part by the Icelandic Research Fund Grant 2410297 and by National Science Centre of Poland Grant 2022/47/B/ST7/00072.

References

[1] T.S. Rappaport, et al., Millimeter wave mobile communications for 5G cellular: It will work!, IEEE Access 1 (2013) 335–349.
[2] T. Rappaport, Y. Xing, G.R. MacCartney, A.F. Molisch, E. Mellios, J. Zhang, Overview of millimeter wave communications for fifth-generation (5G) wireless networks with a focus on propagation models, IEEE Trans. Ant. Propag. 65 (12) (2017) 6213–6230.
[3] Y.-H. Yang, S.-G. Zhou, B.-H. Sun, X.-Z. Gao, Design of wideband circularly polarized antenna array excited by substrate integrated coaxial line for millimeter-wave applications, IEEE Trans. Ant. Propag. 69 (12) (2021) 8943–8948.
[4] W. Hong, K.-H. Baek, S. Ko, Millimeter-wave 5G antennas for smartphones: Overview and experimental demonstration, IEEE Trans. Ant. Propag. 65 (12) (2017) 6250–6261.
[5] T.-L. Zhang, L. Chen, S.M. Moghaddam, A.U. Zaman, J. Yang, Millimeter-wave ultrawideband circularly polarized planar array antenna using bold-C spiral elements with the concept of tightly coupled array, IEEE Trans. Ant. Propag. 69 (4) (2021) 2013–2022.
[6] Z. Pi, F. Khan, An introduction to millimeter-wave mobile broadband systems, IEEE Comm. Mag. 49 (6) (2011) 101–107.
[7] Y. Cheng, Y. Dong, Wideband circularly polarized planar antenna array for 5G millimeter-wave applications, IEEE Trans. Ant. Propag. 69 (5) (2021) 2615–2627.
[8] S. Bhardwaj, N.K. Nahar, J.L. Volakis, Novel phaseless gain characterization for circularly polarized antennas at mm-wave and THz frequencies, IEEE Trans. Ant. Propag. 63 (10) (2015) 4263–4270.
[9] D. Titz, F. Ferrero, C. Luxey, Development of a millimeter-wave measurement setup and dedicated techniques to characterize the matching and radiation performance of probe-fed antennas, IEEE Ant. Propag. Mag. 54 (4) (2012) 188–203.
[10] Y. Yang, B. Sun, J. Guo, A low-cost, single-layer, dual circularly polarized antenna for millimeter-wave applications, IEEE Ant. Wireless Propag. Lett. 18 (4) (2019) 651–655.
[11] W. Hong, K.H. Baek, Y. Lee, Y. Kim, S.T. Ko, Study and prototyping of practically large scale mm-Wave antenna systems for 5G cellular devices, IEEE Comm. Mag. 52 (9) (2014) 63–69.

[12] M. Fakharzadeh, M. Mohajer, An integrated wide-band circularly polarized antenna for millimeter-wave applications, IEEE Trans. Ant. Propag. 62 (2) (2014) 925–929.
[13] J. Wu, Y.J. Cheng, Y. Fan, Millimeter-wave wideband high efficiency circularly polarized planar array antenna, IEEE Trans. Ant. Propag. 64 (2) (2016) 535–541.
[14] D. Muirhead, M.A. Imran, K. Arshad, A survey of the challenges, opportunities, and use of multiple antennas in current and future 5G small cell base stations, IEEE Access. 4 (2016) 2952–2964.
[15] X. Bai, S.-W. Qu, S. Yang, J. Hu, Z.-P. Nie, Millimeter-wave circularly polarized tapered-elliptical cavity antenna with wide axial-ratio beamwidth, IEEE Trans. Ant. Propag. 64 (2) (2016) 811–814.
[16] S. Fakhte, H. Oraizi, R. Karimian, R. Fakhte, A new wideband circularly polarized stair-shaped dielectric resonator antenna, IEEE Trans. Ant. Propag. 63 (4) (2015) 1828–1832.
[17] Y.-M. Cai, K. Li, Y.-Z. Yin, W. Hu, Broadband circularly polarized printed antenna with branched microstrip feed, IEEE Ant. Wireless Prop. Lett. 13 (2014) 674–677.
[18] L. Josefsson, P. Persson, Conformal Array Antenna Theory and Design, Hoboken, NJ, Wiley, USA, 2006.
[19] Y. Yin, B. Zarghooni, K. Wu, Single-layered circularly polarized substrate-integrated waveguide horn antenna array, IEEE Trans. Ant. Propag. 65 (11) (2017) 6161–6166.
[20] H. Yi, Z. Wang, D. Xia, H. Liu, L. Li, Periodic asymmetric trapezoidal perturbation microstrip antenna for millimeter-wave automotive radar sensors, IEEE Trans. Ant. Propag. 71 (2) (2023) 1369–1377.
[21] Y.Q. Guo, Y.M. Pan, S.Y. Zheng, Design of series-fed, single-layer, and wideband millimeter-wave microstrip arrays, IEEE Trans. Ant. Propag. 68 (10) (2020) 7017–7026.
[22] Y. Yin, K. Wu, Endfire circularly-polarized antipodal linearly tapered slot antenna fed by slotted width-tapered SIW, IEEE Trans. Ant. Propag. 70 (4) (2022) 2411–2421.
[23] P.D. Hilario Re, D. Comite, S.K. Podilchak, Single-layer series-fed planar array with controlled aperture distribution for circularly polarized radiation, IEEE Trans. Ant. Propag. 68 (6) (2020) 4973–4978.
[24] W. Lin, R.W. Ziolkowski, T.C. Baum, 28 GHz compact omnidirectional circularly polarized antenna for device-to-device communications in the future 5G systems, IEEE Trans. Ant. Propag. 65 (12) (2017) 6904–6914.
[25] Q. Zhu, K.-B. Ng, C.H. Chan, Printed circularly polarized spiral antenna array for millimeter-wave applications, IEEE Trans. Ant. Propag. 65 (2) (2017) 636–643.
[26] H. Xu, J. Zhou, K. Zhou, Q. Wu, Z. Yu, W. Hong, Planar wideband circularly polarized cavity-backed stacked patch antenna array for millimeter-wave applications, IEEE Trans. Antennas Propag. 66 (10) (2018) 5170–5179.
[27] G. Mishra, S.K. Sharma, J.-C.-S. Chieh, A high gain series-fed circularly polarized traveling-wave antenna at w-band using a new butterfly radiating element, IEEE Trans. Antennas Propag. 68 (12) (2020) 7947–7957.
[28] H. Huang, X. Li, Y. Liu, A low-profile, dual-polarized patch antenna for 5G MIMO application, IEEE Trans. Ant. Propag. 67 (2) (2019) 1275–1279.
[29] Y. Zhang, J. Deng, M. Li, D. Sun, L. Guo, A MIMO dielectric resonator antenna with improved isolation for 5G mm-wave applications, IEEE Ant. Wireless Propag. Lett. 18 (4) (2019) 747–751.